E3S Web of Conferences **677**, 01010 (2025) https://doi.org/10.1051/e3sconf/202567701010
3rd ICDMM 2025

Effect of silt interlayer configuration on the cyclic resistance of loose sand in direct simple shear

Yelvi[1], *A'isyah* Salimah[1*], *Susilawati*[2], *Muhammad* Arif Musyaffa[1], *Handi* Sudardja[1], and *Istiatun*[1]

[1]Department of Civil Engineering, Politeknik Negeri Jakarta, Depok, 16424, Indonesia
[2]Department of Civil and Environmental Engineering, School of Engineering, Monash University Malaysia, Subang Jaya 47500, Malaysia

Abstract. Liquefaction is a major source of earthquake-induced ground failure, especially in loose, saturated sandy deposits common in Indonesia. Understanding how layered soils behave under cyclic loading is therefore crucial for developing effective strategies to mitigate liquefaction. This study evaluates the influence of silt interlayers on the cyclic resistance of loose sand using Cyclic Direct Simple Shear (CDSS) tests. Three configurations were examined at Dr = 40% under fully saturated conditions: pure sand (S), sand–silt–sand (S–M–S), and silt–sand–silt (M–S–M). The hydro-mechanical response is governed by the drainage-barrier behavior of the silt layers, which modifies pore pressure dissipation during cyclic loading. Experimental results show that the presence of silt interlayers substantially accelerates the generation of excess pore-water pressure (r_u) and reduces the number of cycles to liquefaction (NL). Compared with pure sand, cyclic resistance decreased by about 73% for S–M–S and 82% for M–S–M. The highest r_u value (1.096) occurred in the M–S–M configuration, signifying full liquefaction and rapid loss of effective stress. These findings highlight the dominant role of stratigraphic arrangement in liquefaction potential and underscore the importance of identifying thin fine-grained interlayers in hazard assessments for coastal and alluvial deposits.

1 Introduction

Liquefaction is a critical geotechnical hazard in seismically active regions, where saturated, cohesionless soils lose their shear strength due to the buildup of excess pore water pressure during cyclic loading [1, 2]. This phenomenon has caused extensive damage in past earthquakes, including the 2018 Palu event in Indonesia, where widespread liquefaction led to large-scale ground deformation and infrastructure failure. From a disaster mitigation perspective, understanding how pore-water pressure builds up and dissipates is crucial for designing measures such as soil densification, drainage improvement, and foundation reinforcement. Regions with complex stratigraphy, such as sand deposits interlayered with low-permeability silt, pose additional challenges because these layers may influence the distribution and buildup of excess pore pressure during earthquakes. Consequently, laboratory investigations that examine how different stratigraphic configurations respond to cyclic loading provide critical insight for refining liquefaction-hazard assessments and guiding mitigation strategies in vulnerable seismic regions. Within this broader context, the present study aims to clarify the role of thin silt interlayers on the cyclic response of sand, contributing to improved understanding of how subsurface conditions affect liquefaction susceptibility.

As articulated by Terzaghi's principle of effective stress [3], the shear strength of soil is directly governed by the stress transmitted through its granular skeleton. During seismic shaking, the tendency of loose sand particles to rearrange into a denser state under undrained conditions transfers load from the soil skeleton to the pore water, resulting in a rapid increase in excess pore water pressure (EPWP). As EPWP approaches the initial confining stress, the effective stress diminishes, causing the soil to lose nearly all its strength and stiffness and behave like a viscous fluid [4].

Several factors, including the intensity and duration of seismic shaking, and inherent soil properties such as relative density, grain size distribution, and permeability, controlled the susceptibility of a soil deposit to liquefaction [2]. Loose soils (low relative density) are significantly more vulnerable than dense soils because they have a greater potential for contractive behavior under cyclic loading. Similarly, poorly-graded, fine to medium sands are known to be particularly susceptible [5].

While these principles are well-established for clean, homogeneous sands, natural soil deposits are rarely uniform. They are often characterized by complex stratification, including fine-grained interlayers like silt and clay. The influence of these fines has been a subject of considerable debate. Several studies on homogeneously mixed sand-silt specimens report that

* Corresponding author: aisyah.salimah@sipil.pnj.ac.id

© The Authors, published by EDP Sciences. This is an open access article distributed under the terms of the Creative Commons Attribution License 4.0 (https://creativecommons.org/licenses/by/4.0/).

increasing fines content under certain conditions improves liquefaction resistance by altering the soil's intergranular structure [6]. However, more recent evidence shows that the influence of fines is strongly dependent on their stratigraphy. In layered deposits, the stratigraphic positioning of low-permeability fines often has a more significant impact. This is typically an adverse effect on cyclic response, as these layers can impede drainage, promote excess pore pressure buildup, and reduce the overall liquefaction resistance of the soil mass.

It has been hypothesized that thin, low-permeability interlayers embedded within a more permeable sand mass can act as significant drainage barriers [4]. During an earthquake, these layers can impede the upward dissipation of EPWP generated in the underlying sand. This entrapment causes pressure to accumulate much faster and to a higher magnitude than it would in a uniform deposit. A critical consequence of this impeded drainage is the potential formation of a "water film" at the sand-silt interface, which can act as a sliding surface with drastically reduced shear resistance [7]. This mechanism has been validated in large-scale shaking table tests and numerical simulations, which confirm that the presence of a less permeable layer can significantly alter pore pressure distribution, accelerate the onset of liquefaction, and exacerbate ground settlement [8, 9]. Recent laboratory findings by Park et al. [10] further support this, showing that increasing silt layers within a sand specimen consistently decreases its cyclic resistance.

This apparent contradiction in the literature underscores the need to distinguish between the effects of *mixed* soils and *layered* soils. While simplified procedures for liquefaction evaluation based on in-situ tests provide a valuable framework [11], they may not fully capturehe complex effects of thin, but critical, stratigraphic features. Therefore, this study directly addresses this knowledge gap by testing the primary hypothesis: thin, low-permeability silt interlayers within a loose sand deposit will significantly reduce its liquefaction resistance by trapping EPWP.

This research employs a systematic laboratory program using Cyclic Direct Simple Shear (CDSS) tests to achieve this. The CDSS apparatus is particularly well-suited for this investigation as it can best replicate the plane strain conditions and principal stress rotation experienced by a soil element subjected to vertically propagating shear waves during an earthquake [12]. By comparing the detailed cyclic response of homogeneous sand with meticulously prepared layered sand-silt specimens, this study seeks to quantify the impact of different interlayer configurations on the rate of pore pressure generation, shear strain accumulation, and stiffness degradation.

2 Methods

This research methodology is designed as a systematic laboratory experimental program to investigate the influence of silt interlayers on the liquefaction potential of sandy soil. All testing procedures for determining material properties and conducting the CDSS tests adhere to the relevant ASTM standards to ensure reproducibility and validity.

2.1 Materials characterization

Two materials with highly contrasting engineering properties were selected to model a stratified soil system. Their geotechnical properties were thoroughly characterized following relevant ASTM standards to establish a baseline for their behavior.

2.1.1 Lampung Sand

The primary liquefiable material was silica sand from Lampung, Indonesia. Its index properties are summarized in Table 1. The sand's specific gravity (*Gs*) of 2.65 is typical for soils composed primarily of quartz minerals. According to the Unified Soil Classification System (USCS), the material is classified as a poorly graded sand (SP), with a coefficient of uniformity (*Cu)* of 2.06 and a coefficient of curvature (*Cc)* of 0.79. A low Cu indicates that the particle size distribution is relatively uniform. Uniform grading often makes the soil more susceptible to volume reduction and loss of strength under cyclic loading. This inherent instability is a key precondition for liquefaction. The grain size distribution curve (Fig. 1), was plotted on the liquefaction susceptibility chart developed by Tsuchida [5]. The result confirms a high vulnerability to liquefaction. The sand's high permeability ($k \approx 8.25 \times 10^{-2}$ cm/s) is also critical, as it allows for rapid pore pressure generation when drainage is impeded.

Table 1. Index properties of Lampung Sand.

Parameter	Symbol	Value	Unit
Spesific Gravity	G_s	2.65	-
Maximum Void Ratio	e_{max}	0.95	%
Minimum Void Ratio	e_{min}	0.796	%
Effective Diameter	D_{10}	0.18	%
Median Grain Size	D_{50}	0.30	%
Coefficient of Uniformity	C_u	2.06	-
Coefficient of Curvature	C_c	0.79	
Permeability Coefficient	k	$8.25{\times}10^{-2}$	cm/s

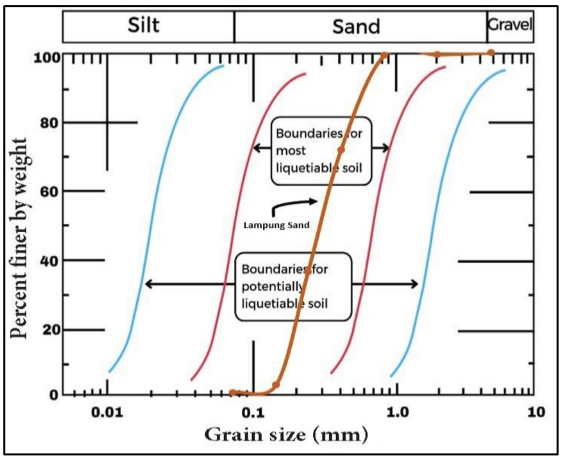

Fig. 1. Gradation curve of Lampung Sand plotted on the liquefaction susceptibility chart by Tsuchida (1970), indicating high susceptibility.

2.1.2 Cikeas Silt

A silt from Cikeas, Indonesia, was used as the interlayer material, and its properties are presented in Table 2. Based on a Liquid Limit (*LL*) of 56.0% and a Plasticity Index (*PI*) of 24.5%, the soil is classified as a high-plasticity silt (MH) according to the USCS. Its position below the A-line on the plasticity chart is typical of inorganic silts. the high plasticity reflects the strong influence of fine particles and their interaction with water, resulting in greater compressibility than sands. The most critical property for this study is the silt's permeability. Falling-head permeability tests yielded a coefficient of permeability (k) of 5.58×10^{-8} cm/s, approximately six orders of magnitude lower than that of the Lampung sand. This contrast in a coefficient of permeability explains the silt layer's role as an effective drainage barrier, a key mechanism investigated in this study.

Table 2. Index properties of Cikeas Silt.

Parameter	Symbol	Value	Unit
Spesific Gravity	G_s	2.67	-
Liquid Limit	*LL*	55.96	%
Plastic Limit	*PL*	31.50	%
Plasticity Index	*PI*	24.46	%
% Finer than No. 200 Sieve	% Fines	65.5	%
USCS Classification	-	MH	-
Permeability Coefficient	k	5.58×10^{-8}	cm/s

2.2 Specimen preparation

All specimens were reconstituted to a diameter of 69.3 mm and a total height of 25 mm.

1) Sand Layers: The sand layers were prepared using the moist tamping method, which is widely recognized for producing uniform, loose specimens essential for repeatability in liquefaction testing. A small water content (6.7% by weight) was added to provide apparent cohesion, reduce particle segregation, and allow precise control of the target relative density.
2) Silt Layers: The silt layers were compacted to match their in-situ bulk density (1.60 g/cm³) and water content (41.5%), ensuring that the interlayer properties reflect field conditions.

Three stratigraphic configurations were prepared to isolate the effect of silt interlayers, as illustrated in Figures 2–4:

a) Sample S (Sand): A homogeneous specimen consisting entirely of Lampung sand (25 mm high), serving as the baseline reference.
b) Sample S-M-S (Sand–Silt–Sand): A three-layer specimen comprising a central 5 mm silt layer between two 10 mm sand layers.
c) Sample M-S-M (Silt-Sand-Silt): A three-layer specimen with a 15 mm thick sand layer confined between two 5 mm silt layers.

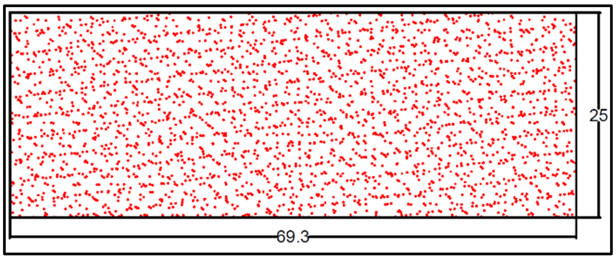

Fig. 2. Schematic of homogeneous sand specimen (S), with dimensions in mm

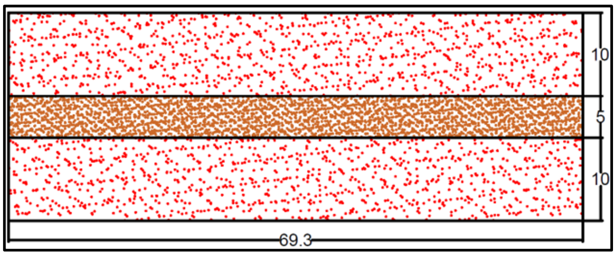

Fig. 3. Of Sand–Silt–Sand specimen (S-M-S), with dimensions in mm.

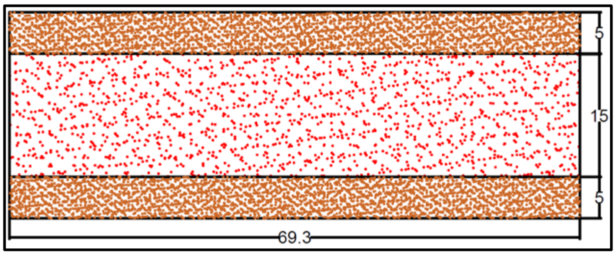

Fig. 4. Schematic of Silt–Sand–Silt specimen, with dimensions in mm.

2.3 Cyclic Direct Simple Shear (CDSS) testing protocol

All tests were performed using a GDS Electromechanical Dynamic Cyclic Simple Shear (EMDCSS) apparatus following ASTM D8296–19. The procedure consisted of three stages:

1. Saturation: Specimens were saturated by flushing with de-aired water under a slight back pressure until Skempton's B-value exceeded 0.95.
2. Consolidation: Specimens were consolidated isotropically to a target effective vertical stress (σ'_{vc}) of 50 kPa. This stress level simulates the in-situ conditions at a shallow depth of approximately 2.5-3.0 meters.
3. Cyclic Shearing: After consolidation, drainage valves were closed, and specimen height was held constant to simulate undrained conditions. A sinusoidal cyclic shear stress was applied at 0.1 Hz. Changes in vertical stress required to maintain constant volume were monitored and used to compute the excess pore pressure ratio ($r_u = \Delta\sigma'_v / \sigma'_{vc}$).

Testing continued until liquefaction occurred, defined as $r_u \geq 0.9$. The selection of a failure criterion based on strain or pore pressure can influence the interpretation of liquefaction resistance [13]. The value of $r_u \approx 1$ is commonly adopted as the threshold for the onset of significant strength loss, while a double-amplitude shear strain is also widely used as a criterion [14]. In all tests, the double-amplitude shear strain (γDA = 20%) was reached before $r_u \approx 1$, indicating that strain based failure was triggered earlier than pore pressure based failure.

2.4 Justification of key test parameters

a) Relative Density (Dr ≈ 40%): Selected to represent loose sandy soils, which exhibit high liquefaction susceptibility due to their contractive behavior under cyclic loading.
b) Effective Vertical Stress (σ'_{vc} = 50 kPa): This stress level simulates a shallow depth of approximately 2.5–3.0 meters. This zone is often highly vulnerable to liquefaction and its surface manifestations, making it a particularly relevant depth for investigation.
c) Cyclic Frequency (f = 0.1 Hz): While lower than typical earthquake frequencies (1-5 Hz), this frequency was selected for two reasons. First, for fully saturated, undrained sand, the cyclic response is mainly independent of the loading rate in this range. Second, a lower frequency allows for higher-resolution data acquisition, ensuring that the rapid changes in pressure and strain within each cycle are accurately captured.
d) Failure Criterion ($r_u \geq 0.9$): The initiation of liquefaction was defined as the cycle at which r_u reached or exceeded 0.9. While various definitions of liquefaction exist, including those based on strain amplitude, the pore pressure criterion is a robust and widely accepted indicator of the onset of significant strength loss [14]. The selection of a specific failure criterion can influence the exact number of cycles to failure, but the relative performance between samples remains consistent [13].

3 Results

The experimental results are presented objectively, beginning with the consolidation behavior and followed by the cyclic response of the samples. This structure allows for a clear presentation of the data before interpretation in the Discussion section.

3.1 Consolidation behavior

The influence of the layered stratigraphy was evident even during the static consolidation phase. Fig. 5 compares the vertical displacement versus the square root of time for the three specimens during consolidation to 50 kPa. Tables 3 – 5 summarize the settlement data at each configuration test. Comparison of cumulative settlement at each consolidation stage is shown in Table 6.

Table 3. Summary of settlement data for sample S

Increment No.	Vertical Stress (kPa)	Vertical Deformation (mm)	Final Sample Height (mm)
1	10	2.16	22.83
2	25	3.16	21.83
3	50	4.13	20.86

Table 4. Summary of settlement data for sample S-M-S

Increment No.	Vertical Stress (kPa)	Vertical Deformation (mm)	Final Sample Height (mm)
1	10	1.70	23.29
2	25	2.98	22.01
3	50	4.36	20.63

Table 5. Summary of settlement data for sample M-S-M

Increment No.	Vertical Stress (kPa)	Vertical Deformation (mm)	Final Sample Height (mm)
1	10	3.58	21.41
2	25	4.46	20.53
3	50	5.97	19.02

Table 6. Comparison of settlement at each consolidation stage

Sample Code	Settlement at 10 kPa (mm)	Cumulative Settlement at 25 kPa (mm)	Final Cumulative Settlement at 50 kPa (mm)
S	2.16	3.16	4.13
S-M-S	1.70	2.98	4.46
M-S-M	3.58	4.36	5.97

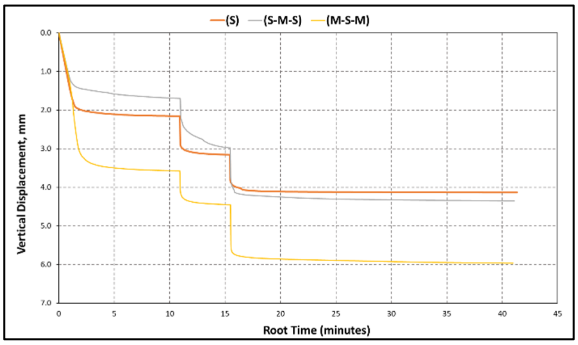

Fig. 5. Comparison of vertical displacement versus the square root of time for the three sample configurations during consolidation

Figure 5 illustrates the vertical displacement versus the square root of time for the three specimens during consolidation under 50 kPa. As summarized in Table 6, the M–S–M configuration exhibited the greatest settlement (5.97 mm), followed by S–M–S (4.46 mm) and S (4.13 mm), reflecting the higher compressibility of the silt layer. The layered specimens also displayed slower consolidation rates, most notably in M–S–M, indicating that the low-permeability silt layers were already restricting vertical drainage prior to cyclic loading. This early manifestation of impeded pore-water dissipation supports the underlying hypothesis regarding the drainage-barrier effect of the interlayer.

3.2 Cyclic response and liquefaction failure

The cyclic behavior of each specimen revealed distinct differences in hydro-mechanical response. Figures 6 and 7 present the evolution of excess pore-water pressure and shear strain accumulation, respectively. To support these graphical trends, Table 10 summarizes the key liquefaction parameters derived from the cycle-by-cycle data presented in Tables 7, 8, and 9.

Table 7. CDSS test data for clean sand sample (S)

N	Cyclic Load (kN)	Cyclic Stress (kPa)	γ_{cyclic} (%)	$\gamma_{permanent}$ (%)	γ_{DA} (kPa)	Δu_{cyclic} (kPa)	$\Delta u_{permanent}$ (kPa)	$\Delta u_{maximum}$ (kPa)	γ_u (-)
1	0.0470	12.5	0.247	-0.523	0.494	6.79	11.82	13.41	0.268
2	0.0450	11.9	0s.592	-2.105	1.184	19.38	22.43	25.61	0.512
3	0.0475	12.6	4.001	-6.573	8.002	29.32	28.53	38.33	0.767
4	0.0465	12.3	8.227	-11.479	16.455	33.43	31.71	43.37	0.867
5	0.0450	11.9	11.272	-16.153	22.544	34.49	32.77	44.17	0.883
6	0.0445	11.8	13.911	-19.782	27.823	35.02	33.83	44.43	0.889
7	0.0430	11.4	15.709	-23.105	31.419	35.29	34.36	44.43	0.889
8	0.0450	11.9	18.301	-26.907	36.602	35.02	34.09	44.43	0.889
9	0.0485	12.9	21.466	-30.560	42.935	35.42	34.62	44.70	0.894
10	0.0420	11.1	22.314	-33.413	44.628	36.74	35.95	44.70	0.894
11	0.0495	13.1	25.646	-36.568	51.292	36.35	35.95	45.23	0.905

Table 8. CDSS test data for S-M-S

N	Cyclic Load (kN)	Cyclic Stress (kPa)	γ_{cyclic} (%)	$\gamma_{permanent}$ (%)	γ_{DA} (kPa)	Δu_{cyclic} (kPa)	$\Delta u_{permanent}$ (kPa)	$\Delta u_{maximum}$ (kPa)	γ_u (-)
1	0.04	10.9	7.022	-12.513	14.045	14.21	24.81	28.53	0.571
2	0.04	11.4	12.719	-19.768	25.439	34.76	31.71	43.37	0.867
3	0.04	9.7	14.239	-25.954	28.477	37.14	33.56	46.55	0.931
4	0.04	10.1	17.292	-29.718	34.584	37.54	34.36	46.55	0.931
5	0.04	11.5	21.605	-34.739	43.210	38.86	34.89	46.82	0.936
6	0.04	11.7	24.886	-38.228	49.772	39.13	33.83	47.35	0.947

Table 9. CDSS test data for M-S-M

N	Cyclic Load (kN)	Cyclic Stress (kPa)	γ_{cyclic} (%)	$\gamma_{permanent}$ (%)	γ_{DA} (kPa)	Δu_{cyclic} (kPa)	$\Delta u_{permanent}$ (kPa)	$\Delta u_{maximum}$ (kPa)	γ_u (-)
1	0.04	11.4	0.589	-0.883	1.178	18.98	32.77	38.07	0.761
2	0.04	11.9	6.216	-4.048	12.432	33.70	40.19	45.49	0.910
3	0.04	11.4	9.696	-4.742	19.392	36.08	43.11	46.55	0.930
4	0.04	11.8	13.005	-5.819	26.011	36.88	43.64	47.08	0.942
5	0.04	10.3	14.730	-5.015	29.459	38.33	43.64	47.35	0.947
6	0.04	10.5	16.974	-3.722	33.948	38.33	42.84	47.35	0.947
7	0.04	10.9	19.532	-2.108	29.063	38.86	42.31	47.35	0.947

Table 10. Summary of key CDSS test results

Key Parameter	Sample S (Sand)	Sample S-M-S (Sand-Silt-Sand)	Sample M-S-M (Silt-Sand-Silt)
Number of Cycles to Liquefaction (N_L)	11	3	2
Reduction in Cyclic Resistance	-	72%	82%
Maximum Pore Pressure Ratio (γ_u)	0.905	0.947	0.947

Table 10 summarizes the key quantitative results of the study and provides a basis for directly comparing the cyclic performance of the three specimens. The Number of Cycles to Liquefaction (N_L) offers the most direct measure of cyclic resistance, with values of 11, 3, and 2 cycles reflecting the strong influence of the silt interlayers. The reduction in cyclic resistance of 73% for S-M-M and 82% for M-S-M demonstrates the strong influence of the silt interlayers. These results indicate that stratigraphic configuration is a dominant factor in liquefaction susceptibility.

3.3 Baseline response: Homogeneous sand (Sample S)

The homogeneous sand specimen serves as the reference case for evaluating the performance of the layered samples. Under cyclic loading, Sample S exhibited a slow and systematic reduction in resistance. The pore pressure ratio (r_u increased incrementally, requiring 11 cycles to reach the liquefaction threshold of $r_u \geq 0.9$ (Fig. 6). Shear strains remained small during the early cycles, with noticeable deformation developing after the ninth cycle as the soil entered a contractive state (Fig. 7). The stress–strain hysteresis loops (Fig. 8) illustrate this behavior: the initial loops are steep and narrow, reflecting high stiffness, and they gradually rotate and widen with continued loading, indicating stiffness degradation and increased energy dissipation.

3.4 Accelerated failure: Single silt interlayer (Sample S-M-S) pore pressure generation

Introducing a 5 mm silt layer in the S–M–S configuration substantially changed the cyclic response. Compared with the homogeneous sand, the specimen exhibited a much faster rate of pore-pressure buildup, reaching $r_u \geq 0.9$ within three cycles (Fig. 6). This rapid hydraulic response corresponded with an early onset of mechanical degradation. Significant shear strains developed from the first cycle and exceeded 20% shortly thereafter (Fig. 7). The hysteresis loops (Fig. 9) reflect this behavior: by the second cycle, the loops had already widened and flattened markedly, indicating pronounced stiffness loss and a substantial reduction in shear resistance.

3.5 Critical failure scenario: Encased sand (Sample M-S-M)

The M–S–M configuration, in which two silt layers fully enclose the sand layer, exhibited the most severe response. Liquefaction initiation ($r_u \geq 0.9$) occurred within only two cycles (Fig. 6), indicating a very rapid buildup of excess pore pressure. The mechanical response followed a similar trend, with large shear strains developing almost immediately after loading began (Fig. 7). The hysteresis loops (Fig. 10) reflect this behavior: after the first cycle, the loops had already flattened substantially, signifying pronounced stiffness degradation. Following this point, the specimen exhibited minimal resistance to further deformation.

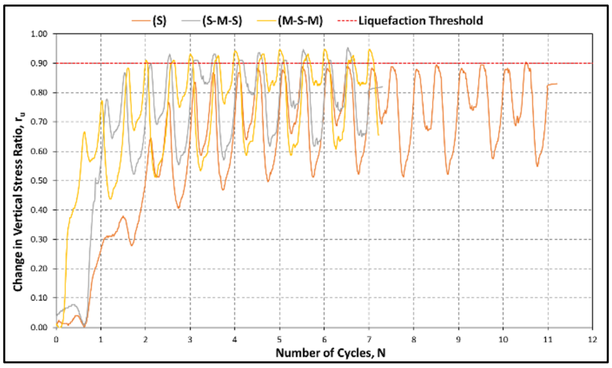

Fig. 6. Comparison of Excess Pore Pressure Ratio (r_u) Generation Versus Number of Cycles (N) for the Three Sample Configurations

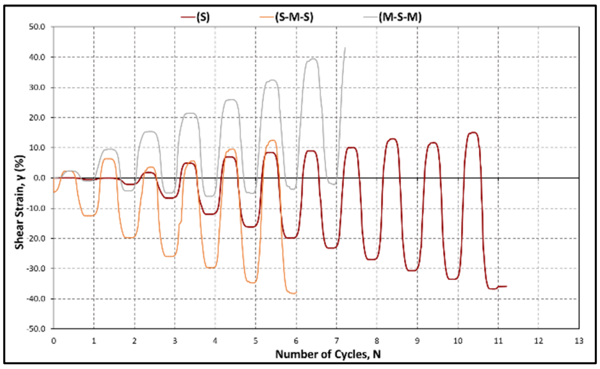

Fig. 7. Comparison of double-amplitude shear strain (γ_{DA}) accumulation versus number of cycles (N) for the three sample configurations

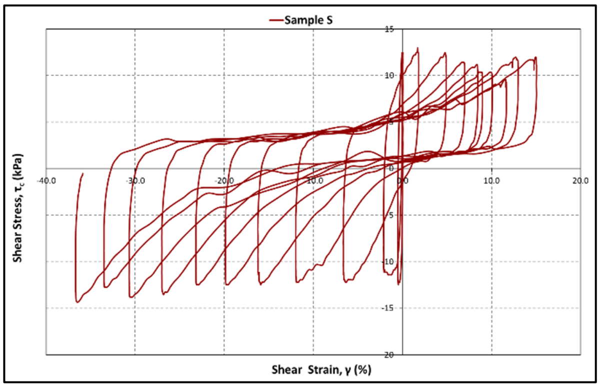

Fig. 8. Representative stress-strain hysteresis loops for each sample type: sand (S) sample.

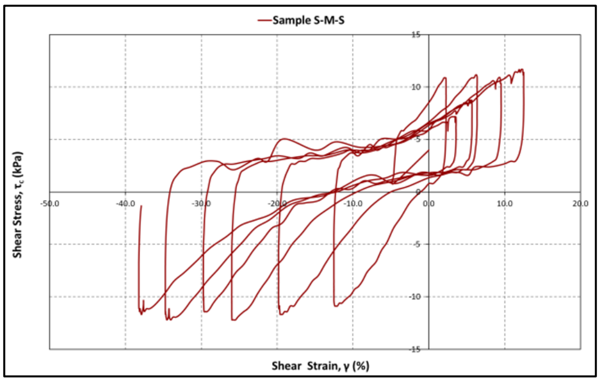

Fig. 9. Representative stress-strain hysteresis loops for each sample type: Sand-Silt-Sand (S-M-S) sample.

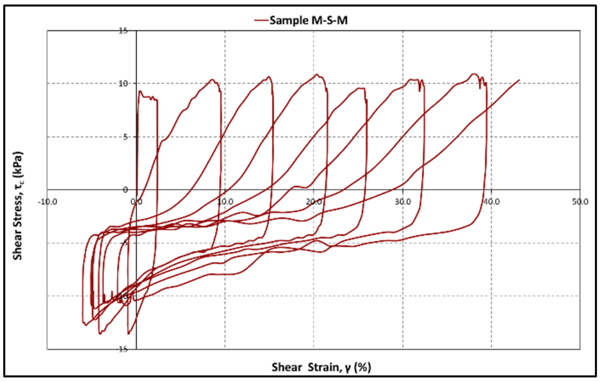

Fig. 10. Representative stress-strain hysteresis loops for each sample type: Silt-Sand-Silt (M-S-M) sample

4 Discussion

4.1 The drainage barrier mechanism: Interpretation of hydro-mechanical coupling

The experimental results provide strong evidence supporting the drainage-barrier hypothesis. The number of cycles to liquefaction (N_L) serves as a direct indicator of cyclic resistance. As shown in Table 10, the inclusion of a single silt layer reduced resistance by 72% in the S–M–S configuration, whereas enclosing the sand with two silt layers reduced resistance by 82% in the M–S–M configuration.

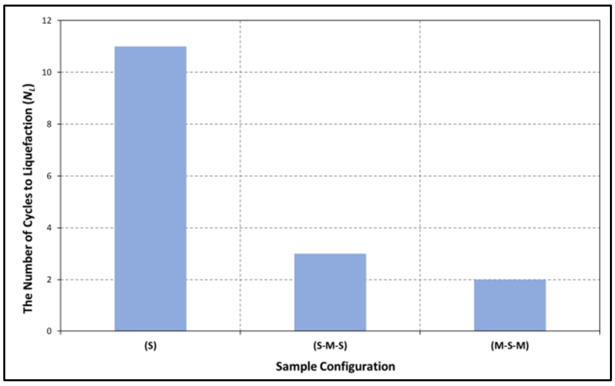

Fig. 11. Bar chart comparing the number of cycles to liquefaction (N_L) for the three sample configurations.

This reduction reflects the hydro-mechanical interaction imposed by the stratigraphy. In the homogeneous sand specimen, excess pore water pressure (EPWP) generated during cyclic loading can dissipate relatively freely. In contrast, the silt interlayers, whose permeability is six orders of magnitude lower than the sand, act as low-permeability boundaries that restrict vertical drainage. As a result, the pore pressure generated within the sand layer becomes confined, causing ru to increase rapidly. According to the effective stress principle, this reduction in effective stress leads to a diminished ability of the sand to resist shear. The close correspondence between the rapid increase in ru (Fig. 6), the early development of large shear strains (Fig. 7), and the stiffness degradation (Fig. 11) is consistent with this mechanism. These observations also align with shake-table and centrifuge studies that reported "water film" formation beneath low-permeability layers, leading to significant strength loss [7, 8].

The M-S-M configuration produced the most severe response because the sand layer was confined above and below by low-permeability silt, providing minimal pathways for dissipation of EPWP. This behavior is consistent with post-earthquake observations in the field, where severe liquefaction effects such as sand boils are often associated with sites capped by silt or clay layers overlying liquefiable sand. The M-S-M sample is a direct laboratory analogue of this hazardous field condition [11].

In all tested configurations, the double-amplitude shear strain (γDA) of 20% was attained earlier than the pore pressure ratio criterion (ru ≈ 1), indicating that substantial deformation and stiffness degradation can precede complete loss of effective stress. This observation is consistent with findings from recent centrifuge and field investigations, which show that shear strain-based thresholds often identify the onset of damaging soil behavior sooner than pore pressure-based criteria [14, 15]. In layered deposits, the early attainment of the strain criterion is particularly significant, as it suggests that large deformations and, consequently, serviceability failures may occur before complete liquefaction is achieved. Such behavior was also noted in earthquake case histories, where structures experienced severe tilt or settlement despite only partial pore pressure buildup (Brandenberg et al., 2020). These results emphasize the importance of considering pore pressure and strain-based criteria in evaluating liquefaction, particularly for stratified soils where drainage impediments can significantly accelerate the deformation response.

These findings are consistent with studies by Ecemis [8], which also identified the detrimental effect of layered heterogeneity. The results do not contradict studies showing increased resistance in *sand-silt mixtures* [6]. Instead, they demonstrate that the *spatial arrangement* of the soils is a more dominant factor than their mere presence. When concentrated into a thin, continuous layer, a small percentage of fines can be far more dangerous than a larger percentage of fines mixed homogeneously within the sand matrix.

4.2 Implications for geotechnical practice

The findings have significant practical implications for liquefaction hazard assessment, particularly in regions such as Indonesia, where alluvial and coastal deposits are common. Standard liquefaction potential assessments, often based on simplified soil profiles from SPT or CPT data, may treat sand deposits with thin fine-grained interlayers as homogeneous. This study clearly shows that such an approach can be dangerously unconservative. The presence of thin, often overlooked, silt or clay layers can be the controlling factor in the liquefaction response of a soil deposit. Therefore, site investigation programs must be designed to meticulously identify and characterize such interlayers, as they can create a liquefaction hazard far greater than predicted for the sand alone.

5 Conclusion

This laboratory study, using Cyclic Direct Simple Shear tests, investigated the influence of low-permeability silt interlayers on the liquefaction potential of loose sand. Based on the experimental results, the following conclusions are drawn:

1. The presence of thin silt interlayers drastically reduces the liquefaction resistance of loose sand deposits. Compared to a baseline of 11 cycles for homogeneous sand, layered samples with one (S-M-S) and two (M-S-M) silt layers failed in only 3 and 2 cycles, respectively.
2. The governing mechanism is the function of the silt layer as a drainage barrier. This barrier traps cyclically induced excess pore water pressure within the sand,

leading to an accelerated loss of effective stress and premature shear failure.
3. The stratigraphic configuration is a first-order control on liquefaction susceptibility. A sand layer fully encased by silt layers (the M-S-M configuration) creates the most efficient pressure trap, thus representing the most hazardous scenario.
4. The findings are a critical reminder for geotechnical practice that liquefaction assessments must move beyond simplified, homogeneous assumptions. Meticulous characterization of soil stratigraphy is paramount for accurately evaluating seismic hazards in layered deposits.

The authors express their sincere gratitude to PT. Hydrocore Indonesia for providing access to advanced laboratory facilities and for their invaluable technical support during the CDSS testing program. This research was financially supported through the PIT UP2M funding scheme of Politeknik Negeri Jakarta and logistically supported by the Department of Civil Engineering, Politeknik Negeri Jakarta.

References

1. I. M. Idriss and R. W. Boulanger, Soil Liquefaction During Earthquakes, (Oakland: Earthquake Engineering Research Institute, 2008)
2. S. L. Kramer, Geotechnical Earthquake Engineering, (New Jersey: Prentice-Hall, 1996)
3. K. Terzhagi, R. B. Peck, and G. Mesri, Soil Mechanics in Engineering Practice, 3rd Edition, (New York: John Wiley and Sons, Inc., 1996)
4. K. Ishihara, Stability of natural deposits during earthquakes, Proceedings of the 11th International Conference on Soil Mechanics and Foundation Engineering, **1**, 321–376, (1985). https://www.issmge.org/uploads/publications/1/34/1985_01_0007.pdf
5. Tsuchida, H., Hayashi, S., and United States-Japan Cooperative Program in Natural Resources Panel on Wind and Seismic Effects, Estimation of liquefaction potential of sandy soils, (McGraw-Hill Company, 4, 91-109, 1971)
6. C. P. Polito and J. R. M. II, Effects of Nonplastic Fines on the Liquefaction Resistance of Sands, Journal of Geotechnical and Geoenvironmental Engineering. **127**(5), (May 2001). https://doi.org/10.1061/(ASCE)1090-0241(2001)127:5(408)
7. T. Kokusho, Water Film in Liquefied Sand and Its Effect on Lateral Spread. J. Geotech. Geoenviron. Eng. **125**(10), 817–826 (1999). https://doi.org/10.1061/(ASCE)1090-0241(1999)125:10(817)
8. N. Ecemis, Experimental and Numerical Modeling on the Liquefaction Potential and Ground Settlement of Silt-interlayered Stratified Sands. Soil Dynamics and Earthquake Engineering. **144,** 106691, (2021). https://doi.org/10.1016/j.soildyn.2021.106691
9. A. Jain, S. Mittal, S. K. Shukla, Energy-based Approach to Study Liquefaction Triggering in Homogeneous and Stratified Soils Under Consolidated Undrained Cyclic Loading, Engineering Geology. 321, (2023). https://doi.org/10.1016/j.enggeo.2023.107151
10. S. S. Park, S. W. Woo, T. N. Nguyen, and D. K. L. Tran, Effect of silt uniformity on the liquefaction resistance of sand–silt mixtures. Soils and Foundations. **64**(5), (2024). https://doi.org/10.1016/j.sandf.2024.101507.
11. H. B. Seed and I. M. Idriss, Simplified Procedure for Evaluating Soil Liquefaction Potential. J. Soil Mech. Found. Div. **97**(9), 1249–1273, (1971). https://doi.org/10.1061/JSFEAQ.0001662
12. W. D. L. Finn, D. J. Pickering, and P. L. Bransby, Sand Liquefaction in Triaxial and Simple Shear Tests, J. Soil Mech. Found. Div. **97**(4), 639–659, (1971). https://doi.org/10.1061/JSFEAQ.000157
13. C. P. Polito, The Effect of Failure Criteria on Liquefaction and Pore Pressure Prediction in Non-Plastic Soils. Geotechnics. **5**(2), 446–482, (2025). https://doi.org/10.3390/geotechnics5020027.
14. J. Wu, A. M. Kammerer, M. F. Riemer, R. B. Seed, and J. M. Pestana, Laboratory study of liquefaction triggering criteria, in 13th World Conference on Earthquake Engineering, Vancouver, B.C., Canada (2004)
15. Gardiner E., Stringer M., Cubrinovski M., Rees S., McGann S., Effect of pumice content on the undrained cyclic behaviour of pumiceous soil. Soils and Foundations. **65**(3), (2025). https://doi.org/10.1016/j.sandf.2025.101629